Interaction of Radiation and Free Convection on a Heated Vertical Plate: Experiment and Analysis

B. W. Webb*
Brigham Young University, Provo, Utah

Introduction

NATURAL convection in channels and from isolated vertical plates has received renewed attention in the heat-transfer research community due to its importance in the electronics industry. Research is needed to define the limits of natural convective cooling, and to explore its interaction with other modes of heat transfer, i.e., conduction and radiation.[1] This Note reports on an experimental and analytical study designed to explore the interaction between laminar free convective and radiative transport from an isolated vertical plate with isoflux heating.

A body of literature reports on combined radiation and natural convection, much of which draws from the similarity solution of Sparrow and Gregg[2] for purely free convective flow from a vertical plate with isoflux heating. The majority of the work in this area has focused on volumetric radiation effects and their interaction with the buoyancy-driven flow and heat transfer from a vertical plate (Arpaci,[3] Hasegawa et al.,[4] Cheng and Özişik,[5] Bankston et al.,[6] Cess,[7] Audunson and Gebhart,[8] and Cess[9]). Additionally, these studies have examined free convection-radiation interaction from vertical plates with constant temperature boundary conditions. The radiative and convective modes of heat transfer are coupled more intimately with isoflux heating, since the local plate temperature is determined by the combined influence of radiation and free convection, whose intensity is in turn determined by the local wall temperature. Only two previous studies, those of Audunson and Gebhart[8] and Cess,[9] address the problem of isoflux heating from isolated vertical plates.

The purpose of this study is to present an analysis of buoyancy-driven free convection from an isoflux vertical plate, coupled to radiation through the thermal boundary condition. Experiments were formulated and carried out to validate the model, and to provide physical understanding of the problem. Model predictions are also compared to the analysis presented by Cess[9] in order to illustrate the areas where the perturbation technique deviates from the solution presented here.

Analysis

Consider a radiatively gray isolated vertical plate of emissivity ε and uniformly imposed heat flux q_w immersed in a nonabsorbing fluid. The heated plate is cooled by free convection and radiation to the freestream fluid and surroundings that are both assumed to be T_∞. Flow and heat transfer are assumed to be two-dimensional and laminar and the Boussinesq approximation is assumed valid. The partial differential equations governing the parabolic free convective flow and heat transfer are given elsewhere[9] and need not be repeated here. It is instructive, however, to restate the thermal boundary condition through which the radiation interaction is felt. At the heated wall ($y = 0$) the thermal boundary condition valid for all axial positions, x, is specified as

$$k\frac{\partial T}{\partial y} = -q_w + \varepsilon\sigma(T^4 - T_\infty^4) \tag{1}$$

The heat flux imposed at the plate surface q_w is dissipated by both convection and radiation.

Previous approaches to the solution of the problem outlined in the foregoing have been that of defining a stream function in the usual manner, and seeking a similarity solution in terms of that stream function and the similarity parameter. For example, Cess[9] proposed a solution for the stream function and the temperature rise in terms of the conventional boundary-layer similarity variable, $\eta = (y/x)(Gr_x^*/5)^{1/5}$, and a new variable, $\xi = (\varepsilon\sigma T_\infty^3/k)(5kv^2x/g\beta q_w)^{1/5}$, which describes the level of interaction between the free convection and radiation heat transfer. Higher order terms were neglected and, hence, the solution is valid only for small and large values of the interaction parameter ξ, respectively. The approach taken here is that of numerical solution. The boundary-layer solution technique of Patankar and Spalding[10] was adopted. The solution technique is well established and has been used to solve a wide variety of boundary-layer flow and heat-transfer problems. Hence, the description of the method that follows is very brief. The technique transforms the conventional x-y coordinates to x-ω, where ω is the fraction of total mass flow in the boundary layer in each flow "tube," and is defined as

$$\omega = \psi/\psi_t \tag{2}$$

where ψ_t is the value of the stream function (or total mass flow rate) at the edge of the boundary layer, and increases as fluid is entrained along the plate length. The usual definition of the stream function is employed. The Patankar-Spalding method is a marching scheme. The solution procedure begins at $x = 0$ and marches along the length of the plate.

A grid-size study was performed to determine the number of cross-stream nodes and the axial step size required to achieve grid-independent results. The final computations reported here were performed with a nonuniform grid network. Grid points were developed in the ω direction in a power law fashion using 300 nodes, and sucessively larger axial marching steps were used in the x direction with approximately 1500 nodes. The selected grid distribution yielded predicted local Nusselt numbers which agreed with the analytical solution of Sparrow and Gregg[2] for the case of negligible radiation coupling ($\varepsilon = 0$) to within 0.1%.

The thermal boundary condition at the heated plate surface, Eq. (1), is expressed as a nonlinear function of surface temperature, which for uniformly imposed heat flux surfaces is part of the solution. The numerical method employed accommodates only linear functions of wall temperature as conventional boundary conditions of the first, second, or third kind. The thermal boundary condition at the heated wall was linearized and expressed in the form

$$k\left.\frac{\partial T}{\partial y}\right|_{y=0} = -(q_w + \varepsilon\sigma T_\infty^4) + (\varepsilon\sigma T_w^{*3})T_w \tag{3}$$

where T_w^* is the wall temperature at the previous axial location. The sensitivity of the calculations to this linearization was assessed by monitoring the difference in surface temperature between adjacent axial nodes. With the grid distribution employed, the absolute heated wall temperatures changed by no more than 0.01% from one axial location to the next. Hence, the procedure yielded results virtually independent of the linearization technique used in the boundary condition.

Received Oct. 4, 1988; revision received Jan. 9, 1989.

*Assistant Professor, Department of Mechanical Engineering.

Experiments

Experimental Apparatus

A schematic of the physical apparatus used in the experiments is shown in Fig. 1. A 32.4 cm length of 0.00254 cm thick 302 stainless steel shim stock was epoxied to a 0.159 cm thick substrate of phenolic material similar to that used in the electronics industry for printed circuit boards. The heater length in the (vertical) flow direction was $L = 15.2$ cm. The stainless steel foil was firmly sandwiched between copper bus bars of 0.95 cm square cross section, which ran the full length of the plate in the vertical direction. The back face of the heated surface was insulated by mounting the heater and phenolic assembly on a 20.3 cm thick substrate of closed-pore extruded polystyrene. Electrical bus bars were embedded flush in the polystyrene.

Power was supplied to the heater with a dc source with voltage and current regulation stable to 0.01%. The Ohmic dissipation in the foil was determined from the voltage-current product measured at the heated surface. The current was displayed directly by the power supply, while the voltage drop was measured with small voltage taps attached electrically to the foil. The Ohmic dissipation rate was thus measured with an expected accuracy of 1%. However, as will be shown subsequently, conjugate effects in the foil and phenolic and polystyrene substrates make it difficult to determine the imposed local heat flux at the heater surface.

Two extremes of the radiative emissivity were studied experimentally, and were achieved by altering the surface condition of the heated foil. A low value of ε was used by polishing the stainless steel to remove contaminants and major scratches. A near-black surface was achieved by painting the heating foil with a very thin coating of flat black lacquer paint. Radiative property data taken from the literature[11] for the two radiative extremes described in the foregoing and corroborative measurements made using infrared radiometry yielded approximate values of the emissivity $\varepsilon = 0.2$ and 0.9 for the polished and blackened surfaces, respectively.

Thermocouples were attached to the heated foil at equal 0.508 cm spatial intervals through holes drilled in the phenolic board along a vertical line midway between the horizontal extremities of the heater. The holes were drilled with a numerically controlled mill to ensure accurate location of the temperature measurements. The thermocouples were fabricated from fine (0.0127 cm diam) copper-constantan thermocouple wire, and were attached directly to the back surface of the heated foil with epoxy. A transient heating experiment was conducted prior to the present study to investigate the possibility of electrical interaction and dc current noise in the thermocouple signal. With the thermocouples attached to the foil heater as described above, a dc voltage was impulsively applied. The emf generated by the thermocouple was monitored using an oscilloscope. The transient response of the thermocouple was a smooth, monotonic trace characteristic of unsteady heating. There was no perceptible "spike" in the response that would be expected if dc current noise were significant. Hence, no dc noise correction was applied to the thermocouple measurements. Additional thermocouples attached to the heated surface 8.1 cm to either side of the centerline instrumentation revealed that the maximum measured horizontal temperature variation was less than 3%. Thermocouples were also placed at the rear of the polystyrene insulation substrate to assess and correct for conduction losses.

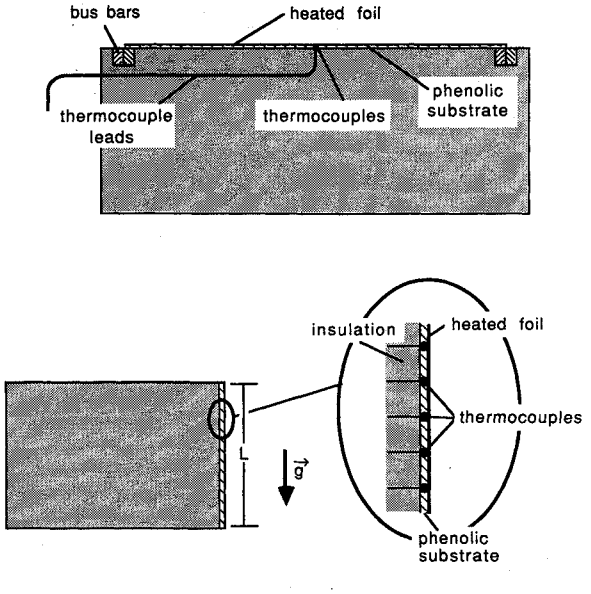

Fig. 1 Schematic diagram of the experimental apparatus: a) plan view, b) side view.

The experiments were performed with air as the working fluid. The entire heater apparatus was isolated from the power supply and other instrumentation in a basement laboratory room free of ventilation currents. The ambient temperature strayed less than 0.2°C throughout the 24 h typically required for the heated wall temperatures to cease changing appreciably.

Data Reduction

Local heated wall temperatures were the primary variable measured in the experiments. From these temperatures, and those measured at the back face of the polystyrene insulation, the conduction loss was determined according to a one-dimensional estimate as

$$q_{\text{cond}} = k_{\text{ins}}(T_w - T_i)/L_{\text{ins}} \tag{4}$$

where k_{ins} and L_{ins} are the effective thermal conductivity and thickness of the composite phenolic/polystyrene substrate and T_i is the temperature measured at the back face of the insulation. The conduction losses were subtracted from the Ohmic dissipation for determining the total imposed heat flux q_w both in calculating local Nusselt numbers and in evaluating the appropriate heat flux input to the model thermal boundary condition [Eq. (1)]. Calculated conduction loss q_{cond} never exceeded 2% of the Ohmic dissipation flux in the foil.

Local convective and radiative components of the heat flux at the heater surface were calculated from the measured temperatures as follows. The local radiative heat flux was determined from the local wall temperature $T_w(x)$ using the relation

$$q_r = \varepsilon\sigma(T_w^4 - T_\infty^4) \tag{5}$$

while the local convective heat flux was simply the difference between the imposed heat flux at the wall (corrected one-dimensionally for conduction losses) and the local radiative flux calculated according to Eq. (5):

$$q_c = q_w - q_r \tag{6}$$

The radiative and convective components of heat transfer were expressed as a fraction of the imposed heat flux at the wall q_w, where q_w was corrected for conduction losses using the estimate outlined in Eq. (4).

Results and Discussion

Two heating rates were employed for each of the radiative surface conditions outlined in the foregoing, 86.0 and 244.0 W/m^2. These are values of the averaged difference be-

tween the Ohmic dissipation and the local conduction loss calculated by Eq. (4). Modified Grashof numbers $Gr^* = g\beta q_w L^4/kv^2$ corresponding to these heating rates were $2.2(10^8)$ and $6.3(10^8)$, well below the established limit for the onset of turbulent free convection.[11] The modified Grashof number was based on thermophysical properties evaluated at the average film temperature $\overline{(T_w + T_\infty)}/2$. The temperature of the surroundings and ambient air was very nearly 22.5°C in all experiments.

Wall Temperature

Figure 2 shows the experimentally observed wall temperature data as normalized by ambient temperature T_∞ for the two different heating rates and two radiative surface conditions studied. Also shown are the model predictions for identical experimental conditions. Calculations for radiatively uncoupled ($\varepsilon = 0$) and radiatively black ($\varepsilon = 1$) surfaces are also shown for comparison. The agreement between model predictions and experimental data is seen to be quite good. Discrepancies are confined to regions near the top and bottom of the heated plate, $x/L = 0$ and 1. The predicted temperatures normalized by T_∞ differ from those measured experimentally by less than 1%. However, this approximate 3°C error, when viewed as a percentage of the local wall temperature rise ($\Delta T = T_w - T_\infty$) of about 15°C near $x/L = 0$, presents a fractional error of nearly 20%. This relatively high percentage error in the local ΔT is most extreme for small wall temperature differences, which occur generally for low heat fluxes, regions near $x/L = 0$, and higher emissivity surfaces. The *average* error in model predictions for the local temperature difference ΔT is approximately 3–4%. This higher error in terms of the local wall temperature rise ΔT (rather than T_w/T_∞) will become significant in the presentation of the heat transfer data. The deviations are believed to be due to two-dimensional conduction effects in the phenolic/insulation substrate, which are most evident at the two streamwise extremes of the heated plate. The agreement between experimental data and model predictions is best near the center of the heated plate, $x/L = 0.4$–0.5. The one-dimensional conduction correction applied to the experimental measurements is unable to remedy the two-dimensional conjugate effects observed.

The experimental and predicted data of Fig. 2 illustrate that the walls are more nearly isothermal for higher surface emissivity. The consequence is that the convective heat-transfer coefficient, although unknown, is more nearly uniform over the surface as radiation effects become important due to higher emissivity.

Local Radiative and Convective Heat Flux

Figure 3 illustrates the predicted and experimentally determined fraction of convective heat flux for the two heating rates and two emissivity extremes studied. Again, agreement is very good between model predictions and experimental data. The maximum discrepancy between prediction and experimental data is 10%, and occurs at small x/L locations for high ε.

The data show that the fraction of convective heat transfer approaches unity for lower emissivity surfaces. The convective heat transfer is approximately 80% for the emissivity 0.2 experiments at both heating rates. The data for $\varepsilon = 0.9$ reveal that the convective heat transfer is below 50% of the imposed wall heat flux over most of the heated surface. Even at the leading edge where the convective heat transfer is expected to be highest, the radiation transport constitutes more than 30% of the total heat transfer for $\varepsilon = 0.9$. Again, it should be underlined that dimensional temperatures in the experimental work were all very low, below 60°C.

Boundary-Layer Temperature Profile

Figure 4 shows model predictions of the dimensionless temperature ϕ in the boundary layer with the experimental data of Audunson and Gebhart,[8] where ϕ has been defined as $\phi = (T_w - T_\infty)/(q_w x/k)(Gr_x^*/5)^{1/5}$, and ξ and η have been defined in the foregoing. Air at moderate pressures was used at the working fluid, and hence, negligible volumetric radiation effects were present. The model predicts the local temperature in the boundary layer very well at both values of the radiation-free convection similarity variable ξ, which correspond to two different surface emissivities. It should be noted, however, that the prediction of the thermal field in the boundary layer is quite forgiving. If the surface temperature T_w is predicted accurately, the calculation of the temperature distribution in the boundary layer follows quite naturally by matching the thermal boundary conditions at $y = 0$ and at $y \to \infty$. The negligible error underlines the model's ability to accurately predict the local wall temperature. This level of agreement is expected with the experiments of Audunson and Gebhart, since conjugate effects were less dominant; radiation and free convection occurred on both sides of the thin heated wall.

Local Nusselt Number

The perturbation solution of Cess[9] resulted in asymptotic distributions of local Nusselt number for small and large values of the radiation-free convection similarity variable,

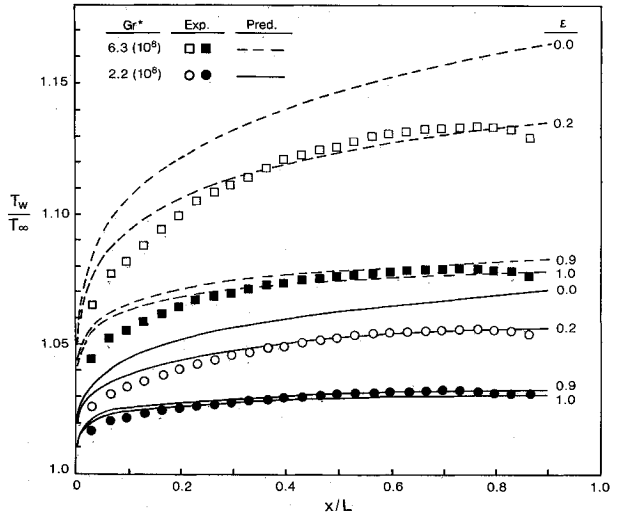

Fig. 2 Predicted and experimentally measured dimensionless wall temperature variation with axial position.

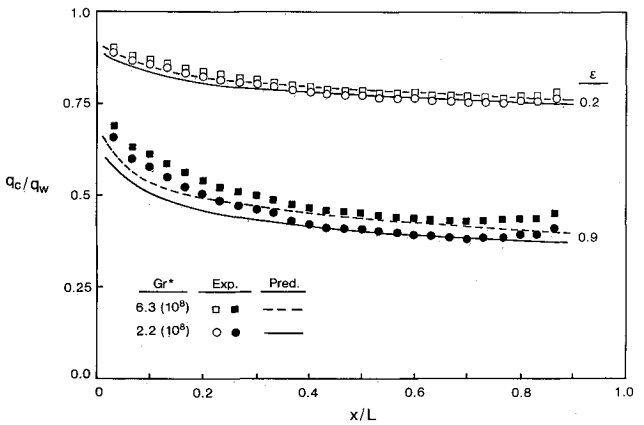

Fig. 3 Predicted and experimentally determined fraction of the imposed wall heat flux dissipated by free convection.

respectively, given by

$$\frac{Nu_x f_q(Pr)}{Gr_x^{1/4}} = 1.0 - 0.396\xi + \cdots \quad (7)$$

and

$$\frac{Nu_x f_g(Pr)}{Gr_x^{1/4}} = 0.877 + 0.0172\xi^{-5/4} + \cdots \quad (8)$$

where the local Grashof and Nusselt numbers have been defined as $Gr_x = g\beta(T_w - T_\infty)x^3/\nu^2$ and $Nu_x = q_c x/k(T_w - T_\infty)$, respectively. Note the presence of factor $f_q(Pr)$ in the ordinate, which accounts for the Prandtl number effect as determined from boundary-layer theory for isoflux heating. The function $f_q(Pr)$ is shown[9] to have a numerical value of 0.407 for $Pr = 0.71$. The relationships given by Eqs. (7) and (8) asymptote to the local Nusselt number distributions for isoflux and isothermal boundary conditions, respectively, for pure free convection in the limiting conditions $\xi \to 0$ and $\xi \to \infty$. The analogous function $f_t(Pr)$ for an isothermally heated plate is 0.357 for $Pr = 0.71$, approximately 12% lower than the corresponding value for isoflux heating. The asymptotic value of $Nu_x f_q(Pr)/Gr_x^{1/4}$ at high ξ is thus 88% of that for low ξ.

Shown in Fig. 5 are model predictions from the present study for the local Nusselt number parameter $Nu_x f_q(Pr)/Gr_x^{1/4}$ vs the similarity variable ξ. In general, the predictions agree

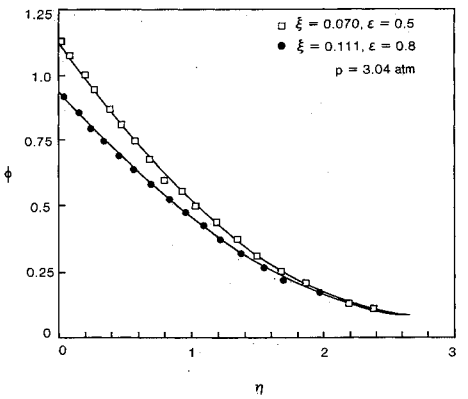

Fig. 4 Predicted temperature profiles in the boundary layer for the experimental data of Audunson and Gebhart[8] at two values of the radiation-free convection interaction parameter ξ.

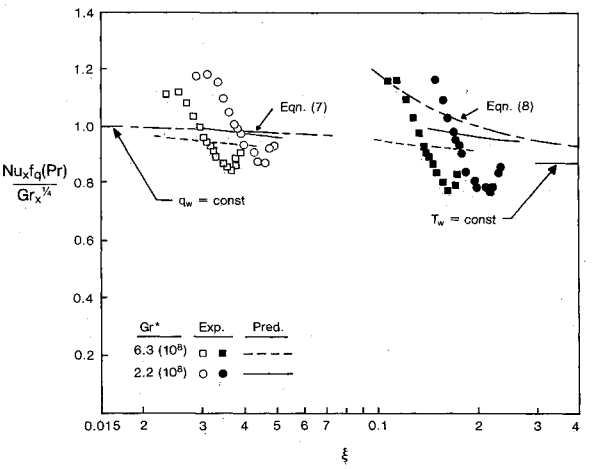

Fig. 5 Comparison of present predictions and experimental data with the local Nusselt number distributions given by the limiting perturbation solutions of Cess.[9]

reasonably well both with the model predictions and the results of the perturbation analysis of Cess.[9] The areas of greatest discrepancy are near the leading and trailing edges of the heated plate, where a maximum deviation of nearly 20% is observed. The strong discrepancy between experimental data and model predictions may be explained as follows. The previously observed error in the local wall temperature rise $T_w - T_\infty$, due to two-dimensional conjugate effects present in the experiments, is amplified in the calculation of the heat transfer parameter $Nu_x/Gr_x^{1/4}$, since ΔT appears raised to the 5/4 power in the denominator. The heat-transfer data near the center of the heated plate where conjugate effects are much smaller agree very well with the results of both analyses. Also in question is the inability of a parabolic model to accurately predict flow and heat transfer near the leading edge of the heated plate; if the first four streamwise data points corresponding to local Grashof numbers below $Gr_x^* \approx 10^4$ are discarded (where the boundary-layer restrictions may be locally violated), the agreement between predictions and experimental data is much better.

The discrepancy between the results of the analysis presented here and that developed by Cess[9] is also illustrated in Fig. 5. The truncation of higher order terms in the perturbation solution results in a failure of the perturbation analysis to correctly predict the local heat-transfer parameter. However, the difference between the two analyses is quite small. The difficulty lies in prescribing the ξ limit of validity of the approximate solutions given by Eqs. (7) and (8). The perturbation solution for small ξ agrees quite well with the predictions of this study; the maximum deviation occurs near $\xi = 0.6$, and is about 4%. However, it may be seen that the perturbation solution fails to predict the detailed local heat-transfer behavior (and hence, wall temperature distribution) for varying heating rates at the two Grashof numbers shown. One would expect the higher order terms truncated to improve the results of the perturbation solution. Indeed, Cess[9] mentions that the parameter $q_w/\varepsilon\sigma T_\infty^4$ would appear in the second term of Eq. (7) had the radiation effect not been linearized.

Conclusions

An experimental and theoretical investigation was conducted to characterize the interaction between radiation and natural convective heat transfer from a single, isolated vertical plate with a uniform heat flux boundary condition and negligible absorption of the fluid. Model predictions show good agreement with the experimental data presented. The results show that radiation coupling renders the heated surface temperature more nearly uniform than without radiation effects ($\varepsilon = 0$). Underlined by both prediction and experiment is the importance of radiation heat transfer in buoyancy-driven flows from vertical plates. Comparisons with previously published perturbation solutions show good agreement in the limiting conditions, and illustrates where these analyses break down.

Acknowledgments

Partial support of this work by the National Science Foundation under Grant CBT-8552493 is gratefully acknowledged. Computer facilities were made available by the BYU CAEDM computer network.

References

[1]Incropera, F. P. (ed.), "Research Needs in Electronic Cooling," Proceedings of a Workshop Sponsored by the National Science Foundation and Purdue University, Andover, MA, 1986.

[2]Sparrow, E. M. and Gregg, J. L., "Laminar Free Convection From a Vertical Plate With Uniform Heat Flux," *ASME Transaction Series C*, Vol. 78, February 1956, pp. 435–440.

[3]Arpaci, V. S., "Effect of Thermal Radiation on the Laminar Free Convection from a Heated Vertical Plate," *International Journal of Heat and Mass Transfer*, Vol. 11, May 1968, pp. 871–881.

[4]Hasegawa, S., Echigo, R., and Fukuda, K., "Analytical and Experimental Studies on Simultaneous Radiative and Free Convective Heat Transfer Along a Vertical Plate," *Proceedings of the Japanese Society of Mechanical Engineers*, Vol. 38, 1972, pp. 2873–2882.

[5]Cheng, E. H. and Özişik, M. N., "Radiation with Free Convection in an Absorbing, Emitting, and Scattering Medium," *International Journal of Heat and Mass Transfer*, Vol. 15, June 1972, pp. 1243–1252.

[6]Bankston, J. D., Lloyd, J. R., and Novotny, J. L., "Radiation-Convection Interaction in an Absorbing-Emitting Liquid in Natural Convection Boundary Layer Flow," *ASME Journal of Heat Transfer*, Vol. 99, February 1977, pp. 125–127.

[7]Cess, R. D., "The Interaction of Thermal Radiation with Free Convection Heat Transfer," *International Journal of Heat and Mass Transfer*, Vol. 9, 1966, pp. 1269–1277.

[8]Audunson, T. and Gebhart, B., " An Experimental and Analytical Study of Natural Convection with Appreciable Radiation Effects," *Journal of Fluid Mechanics*, Vol. 52, March 1972, pp. 57–95.

[9]Cess, R. D., "The Interaction of Thermal Radiation with Conduction and Convection Heat Transfer," *Advances in Heat Transfer*, Vol. 1, edited by T. F. Irvine and J. P. Hartnett, Academic Press, New York, 1964, pp. 1–50.

[10]Patankar, S. V. and Spalding, D. B., *Heat and Mass Transfer in Boundary Layers*, 2nd ed., Intertext Books, London, 1970.

[11]Incropera, F. P. and DeWitt. D. P., *Introduction to Heat Transfer*, Wiley, New York, 1985.

Step Heat Flux Effects on Turbulent Boundary-Layer Heat Transfer

Robert P. Taylor,* Philip H. Love,†
Hugh W. Coleman,‡ and M. H. Hosni†
Mississippi State University,
Mississippi State, Mississippi

Introduction

THIS Note presents heat-transfer data for the case of incompressible turbulent flow of air over a smooth flat plate with an unheated starting length followed by a heated region with a constant wall heat flux. To the authors' knowledge, no experimental data have been reported in the literature for this step heat flux boundary condition. In their definitive work, Reynolds, Kays, and Kline[1] present an integral solution for this case and experimental results for a double-pulse heat flux boundary condition and an arbitrary heat flux boundary condition.

Experiments

A complete description of the facility and its qualification is presented by Coleman et al.[2] This closed-loop air tunnel has a freestream velocity range of 6 to 67 m/s. The air temperature is controlled with a heat exchanger and cooling water loop. A system of honeycomb and screens produces a freestream turbulence intensity at the nozzle exit of less than 0.3%. The thermal boundary condition is set by computer control of the electrical power to each of the 24 individual plates that make up the bottom surface of the nominally 0.1 m high by 0.5 m wide by 2.4 m long test section. Each 0.1 m plate is at a uniform temperature. The top wall of the test section can be adjusted to maintain a constant freestream velocity. The boundary layer is tripped with a 1 mm high by 12 mm wide wooden strip that is located immediately in front of the test surface.

The data reduction expression for the Stanton number is obtained from an energy balance on each test plate as

$$St = \frac{W - q_r - q_c}{A\rho c_p u_\infty (t_w - T_\infty)} \tag{1}$$

Here, W is the electric power to the plate, q_r the radiative heat loss, q_c the conductive heat loss, A the plate area, ρ the air density, c_p the air-specific heat, u_∞ the freestream velocity, t_w the plate temperature, and T_∞ the freesteam stagnation temperature. All properties are evaluated at the freestream static temperature. The details of these measurements and estimation of the uncertainty are given by Love et al.[3] The St uncertainty, U estimates are presented in Tables 1 and 2.

Theories

The classic solution for the step heat input problem was presented by Reynolds, Kays, and Kline.[1] They used the step wall temperature solution of the integral boundary-layer equations as the kernel in a superposition interal to obtain the Stanton number $St(\phi;x)$ for an unheated length ϕ, followed by a constant heat flux as

$$\frac{St_t(x)}{St(\phi;x)} = \frac{\beta_r(1/9,10/9)}{\Gamma(1/9)\Gamma(8/9)} \tag{2}$$

$$r = 1 - (\phi/x)^{0.9}$$

where $St_t(x)$ is the Stanton number for a constant wall temperature without starting length, Γ the gamma function, and β_r the incomplete beta function

$$\beta_r(a,b) = \int_0^r z^{a-1}(1-z)^{b-1}\,dz \tag{3}$$

The results of the experiments are also compared with finite-difference solutions of the partial differential equations of the boundary layer. The solutions presented here are based on a mixing length turbulence model with van Driest damping and a turbulent Prandtl number, $Pr_t = 0.9$. All computations presented were made with the BLACOMP code as verified by Gatlin.[4]

Results

Stanton number measurements were made for six cases ($\phi = 0.3$, 0.7, and 1.3 m at $u_\infty = 28$ m/s and 0.5, 0.8, and 1.3 m at $u_\infty = 67$ m/s). The cases were selected to obtain an appropriate spread in Reynolds numbers, Re_ϕ. The results of these measurements are presented in Tables 1 and 2.

Figure 1 shows a summary of the Stanton number data for a constant heat flux boundary condition and the unheated starting length cases for $u_\infty = 28$ m/s and $u_\infty = 67$ m/s. The figure shows that as the thermal boundary layer develops, the unheated starting length Stanton numbers approach the results for the constant heat flux boundary condition. The first heated plate is highlighted in each case by plotting its data as a solid symbol. Data from the last plate are not plotted for any case. The curve in Fig. 1 is Eq.(2) for $\phi = 0$, $St/St_t = 1.043$, with $St_t = 0.185\ Pr^{-0.4}\ [\log_{10}(Re_x)]^{-2.584}$.[2,3] This St_t expression is the usual $St_t Pr^{0.4} = C_f/2$ with the well-known Schultz-Grunow correlation for C_f.[1]

Received Oct. 21, 1988; revision received Feb. 9, 1989.

*Associate Professor, Thermal & Fluid Dynamics Laboratory, Mechanical and Nuclear Engineering Department. Member AIAA.

†Graduate Research Assistant, Thermal & Fluid Dynamics Laboratory, Mechanical and Nuclear Engineering Department.

‡Professor, Thermal & Fluid Dynamics Laboratory, Mechanical and Nuclear Engineering Department. Member AIAA.